

1 The role of föhn winds in Antarctic Peninsula rapid ice shelf collapse

2 Matthew K. Laffin¹, Charles S. Zender^{1,2}, Melchior van Wessem³, Sebastián Marinsek⁴

3 ¹Department of Earth System Science, University of California, Irvine, USA

4 ²Department of Computer Science, University of California, Irvine, USA

5 ³Institute for Marine and Atmospheric Research Utrecht (IMAU), Utrecht University, Utrecht, Netherlands

6 ⁴Instituto Antártico Argentino, Buenos Aires, Argentina

7 *Correspondence to:* Matthew K. Laffin (mlaffin@uci.edu)

8 **Abstract.** Ice shelf collapse reduces buttressing and enables grounded glaciers to contribute more rapidly to sea-level rise in
9 a warming climate. The abrupt collapses of the Larsen A (1995) and B (2002) ice shelves on the Antarctic Peninsula (AP)
10 occurred while large period ocean swells damaged the calving fronts and the ice shelves were inundated with melt lakes that
11 led to large-scale hydrofracture cascades. During collapse, surface observations indicate föhn winds were present on both ice
12 shelves. Here we use a regional climate model and Machine Learning analyses to evaluate the contributory roles of föhn
13 winds and associated melt events prior to and during the collapses for ice shelves on the AP. Föhn winds caused about 25%
14 \pm 3% of the total annual melt in just 9 days on Larsen A prior to and during collapse and were present during the Larsen B
15 collapse which helped form extensive melt lakes that surpassed a critical stability depth. At the same time the off-coast wind
16 direction created by föhn winds helped melt and physically push sea ice away from the ice shelf calving fronts that allowed
17 large period ocean swells to reach and damage the front, which ultimately triggered collapse. Collapsed ice shelves
18 experienced enhanced surface melt driven by föhn winds over a large spatial extent and near the calving front, whereas
19 extant ice shelves are affected less by föhn wind-induced melt and do not experience regular melt ponds. These results
20 suggest extant ice shelves are less likely to experience rapid collapse due to föhn-driven melt so long as surface temperatures
21 and föhn occurrence remain within historical bounds.

22 1 Introduction

23 The sudden disintegration of ice shelves on the eastern periphery of the Antarctic Peninsula (AP) represents the culmination
24 of a critical regional warming trend and anomalous surface melt in the region (Vaughan et al., 2003). Ice shelves, the floating
25 extensions of grounded glaciers, subdue the discharge of grounded ice into the global ocean (Rignot et al., 2004; Scambos et
26 al., 2004; Gudmundsson et al., 2013; Borstad et al., 2016). Re-examination of past ice shelf collapse events can help to shed
27 light on the mechanisms of collapse and improve the understanding of ice shelf dynamics for future projections of sea-level
28 rise (Rignot et al., 2004; Gudmundsson et al., 2013; Borstad et al., 2016). The final collapses of the Larsen A (LAIS) in 1995
29 and the Larsen B (LBIS) ice shelves in 2002 have been attributed to decreased structural integrity brought on by a

30 combination of factors. Most notably, regional atmospheric warming (Scambos et al., 2000; Mulvaney et al., 2012), extended
31 melt seasons (Scambos et al., 2003), multi-year firn pore space depletion (Kuipers Munneke et al., 2014; Trusel et al., 2015),
32 melt pond flooding and crevasse expansion through hydrofracture (Scambos et al., 2003; Trusel et al., 2013; Pollard et al.,
33 2015; Alley et al., 2018; Banwell et al., 2019; Robel and Banwell, 2019; Leeson et al., 2020), glacier structural
34 discontinuities (Glasser et al., 2008), basal melt (Pritchard et al., 2012; Rignot et al., 2013; Depoorter et al., 2013; Schodlok
35 et al., 2016; Adusumilli et al., 2018), warm melt-water intrusion (Braun et al., 2009), melting of the ice mélange within rifts
36 conducive to rift propagation (Larour et al., 2021), and regional sea ice loss allowing ocean swell flexure stress on the
37 calving front (Banwell et al., 2017; Massom et al., 2018).

38 While the list of mechanisms that can destabilise ice shelves is extensive, a conceptual model for rapid ice shelf
39 collapse proposed by Massom et al., (2018) identifies 4 essential prerequisites for sudden collapse: (1) extensive surface
40 flooding and hydrofracture; (2) reduced sea ice or fast ice at the ice shelf front; (3) outer margin or terminus fracturing and
41 rifting; and (4) initial calving trigger at the ice shelf margin. In addition Massom et al., (2018) concluded that a lack of
42 summer sea ice allowed large period ocean swells to reach the ice shelf calving front. They theorise waves led to calving
43 front damage and small calving events that breached the “compressive arch” of stability of both ice shelves proposed by
44 Doake et al., (1998). At the same time the ice shelves were covered in extensive surface melt lakes that were unlikely to
45 drain horizontally because of the relatively flat surface (Banwell et al., 2014). Satellite observations and ice shelf stability
46 model studies determined the LBIS was covered with >2750 melt lakes that were on average 1 meter deep before collapse
47 which corresponds to a possible melt lake depth stability threshold for ice shelves in the region (Glasser and Scambos
48 (2008); Banwell et al., 2013). Ice shelves inundated with surface melt lakes are susceptible to disintegration through a
49 process known as hydrofracture, where meltwater applies outward and downward pressure to the walls and tip of crevasses
50 that can propagate through the ice shelf (Scambos et al., 2003; Banwell et al., 2013; Bell et al., 2018; Lhermitte et al., 2020).
51 Furthermore, melt lakes at critical water depths can create fracture patterns that split ice shelves into sections with aspect
52 ratios that support unstable rollover, and hydrofracture cascades that begin when melt lakes drain and/or calving occurs at the
53 ice shelf terminus (Scambos et al., 2003; Banwell et al., 2013; Burton et al., 2013; Robel and Banwell (2019)). The
54 combination of ocean swell stress on the calving front and extensive melt ponds led to large scale hydrofracture cascades that
55 proposed by Massome et al., (2018) ultimately caused the rapid collapse of LAIS and LBIS.

56 In addition to a lack of sea ice and extensive melt ponds, meteorological and satellite observations identify clear
57 skies and warm west/northwest föhn wind at the time of collapse (Figure 1b-f) (Rott et al., 1998; Rack and Rott (2004); Cape
58 et al., 2015; Massom et al., 2018). Föhn winds form when relatively cool moist air is forced over a mountain barrier, often
59 leading to precipitation on the windward side of the barrier that dries the air mass (Grosvenor et al., 2014; Elvidge et al.,
60 2015). As the now drier air descends the leeward slope it warms adiabatically and promotes melt directly through sensible
61 heat exchange, and indirectly by the associated clear skies that allow additional shortwave radiation to reach the surface in

62 non-winter months (Turton et al., 2017, 2018; Kuipers Munneke et al., 2018; Elvidge et al., 2020; Laffin et al., 2021). Föhn
63 winds and their capacity to cause surface melt have been studied extensively on the AP. Observations and model studies on
64 the LCIS confirm the föhn mechanism that enhances sensible heat and shortwave radiation and alters local albedo which can
65 increase surface melt rates upwards of 50% compared to non-föhn conditions (Cape et al., 2015; Elvidge et al., 2015; King et
66 al., 2015, 2017; Kuipers Munneke et al., 2012, 2018; Bevan et al., 2017; Lenaerts et al., 2017; Datta et al., 2019;
67 Kirchgaessner, et al., 2021; Laffin et al., 2021, Wang et al., 2021). Late season föhn melt reduces firn pore space, and thus
68 pre-conditions ice shelves to form melt ponds and are responsible for the increased firn density pattern east of the AP
69 mountains on the LCIS (Holland et al., 2011; Kuipers Munneke et al., 2014; Datta et al., 2019). Föhn melt climatology
70 studies have aimed to identify how much melt is caused by föhn and the locations most affected and found föhn winds
71 account for up to 17 % of melt and are concentrated in the LCIS inlets (Turton et al., 2017; Datta et al., 2019; Laffin et al.,
72 2021). Pressure gradient differences across the AP range lead to föhn winds that funnel through mountain gaps as highly
73 concentrated föhn jets, particularly in inlets east of the AP range (Luckman et al., 2014; Elvidge et al., 2015; Kuipers
74 Munneke et al., 2012; Grosvenor et al., 2014). In addition to enhancing surface melt rates, föhn winds exert force on sea/ice
75 ice and drag it away from the calving front, thereby exposing the front to ocean waves (Bozkurt et al., 2018). Climatic
76 studies of the Larsen B embayment indicate that föhn winds were coincident with collapse (Rack and Rott (2004); Leeson et
77 al., 2017). However, it is unknown if concentrated föhn jets spilled onto the former LAIS and LBIS and, if so, whether those
78 föhn winds contributed to their collapse. The questions, therefore, arise: 1) To what extent does föhn-induced melt contribute
79 to the surface melt budget on the AP, specifically LAIS and LBIS?; 2) Did föhn winds and associated melt play a role in
80 triggering the collapses of the LAIS and LBIS?; 3) What are the implications of föhn-induced melt for the remaining eastern
81 AP ice shelves?

82 To address these questions we consider three metrics: Section 3.1 explores the total annual surface melt quantity
83 induced by föhn winds and how melt is spatially distributed across each ice shelf; Section 3.2 identifies the coincidence of
84 föhn-induced melt preceding and during the collapse events, and the estimated melt-lake depth in response to melt events.;
85 Section 3.3 identifies the contribution of föhn melt to the climatological surface liquid water budget comparing collapsed and
86 extant ice shelves. By constructing a timeline of melt and melt mechanisms and comparing melt metrics with collapsed and
87 extant ice shelves, we can identify the contributory factors to collapse.

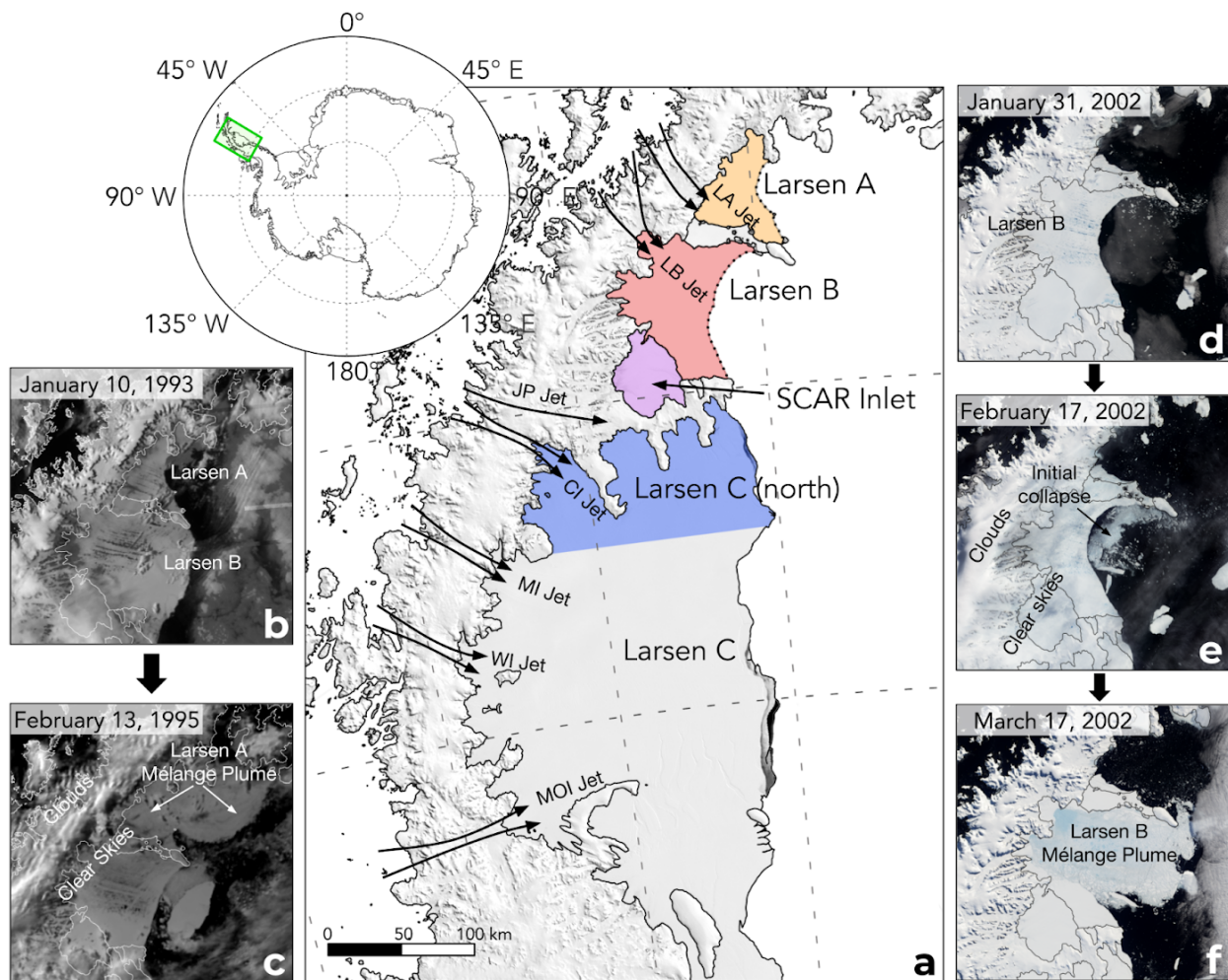


Figure 1. Map of the northern Antarctic Peninsula (a) showing locations of ice shelves and föhn jets (Larsen A jet (LA jet), Larsen B jet (LB jet), Jason Peninsula jet (JP jet), Cabinet inlet jet (CI jet), Mill inlet jet (MI jet), Whirlwind inlet jet (WI jet), Mobil Oil inlet jet (MOI jet)) with a MODIS Mosaic overlay. The colored regions indicate how this study separates ice shelves for climatic analysis. The dotted lines show the former extent of the Larsen A and Larsen B ice shelves at the time of collapse. Panels (b)-(f) are satellite images of the collapses of the LAIS and LBIS. (b) AVHRR (Advanced Very High-Resolution Radiometer) image of the northern AP two years before the collapse of the LAIS showing melt lakes on the surface of both ice shelves. (c) AVHRR image after the collapse of the LAIS. (d) NASA provided MODIS (Moderate Resolution Imaging Spectroradiometer) image showing the LBIS days before collapse began. (e) MODIS image showing a föhn wind event (clouds over the western AP, clear skies over the ice shelves) along with the initial collapse of the LBIS. (f) MODIS image of the complete collapse of the LBIS.

98 **2 Data and methods**

99 **2.1 Regional Climate Model 2 Simulation (RACMO2)**

100 We base our analysis on 3-hourly output from simulations by the Regional Atmospheric Climate Model 2 (RACMO2),
101 version 2.3p2, with a horizontal resolution of 5.5km (0.05°) focused on the AP from 1979-2018. RACMO2 uses the physics
102 package CY33r1 of the ECMWF Integrated Forecast System (IFS)
103 (<https://www.ecmwf.int/en/elibrary/9227-part-iv-physical-processes>\textit{{ECMWF-IFS,} 2008}) in combination with
104 atmospheric dynamics of the High-Resolution Limited Area Model (HIRLAM). RACMO2 has been evaluated against
105 numerous surface observations in locations all over the AP and has trouble simulating very high and low-temperature
106 extremes in the region but is considered a good representation of surface conditions (Leeson et al., 2017; Laffin et al., 2021).

107 **2.2 Föhn wind detection**

108 We use the Föhn Detection Algorithm (FöhnDA) that identifies föhn winds that cause melt using 12 Automatic Weather
109 Stations (AWS) on the AP previously developed and detailed in Laffin et al., (2021). FöhnDA identifies föhn-induced melt
110 events using binary classification Machine Learning when 10 metre air temperature (T) is greater than 0°C, which ensures it
111 captures föhn events that cause surface melt. Thresholds for relative humidity (RH) and wind speed (WS) are more dynamic
112 because high wind speeds and low relative humidity do not guarantee temperatures above freezing, they only aid to identify
113 föhn. FöhnDA uses quantile regression to identify these variable thresholds that take into account the climatology and
114 seasonality at each AWS site. FöhnDA uses two empirically determined thresholds: the 60th percentile wind speed and 30th
115 percentile relative humidity which are 2.85 m/s and 79% averaged at all AWS locations. We co-locate AWS with the nearest
116 model grid cell and use FöhnDA results to train a ML model that detects föhn winds in RACMO2 output. Our ML model
117 improves the accuracy of föhn detection by over 23% when compared to the simple binary classification method applied to
118 RACMO2 output as described above. A sensitivity study detailed in Laffin et al., (2021) compares previous föhn detection
119 methods (Cape et al., 2015; Datta et al., 2019) and shows that FöhnDA is the most accurate detection method and allows us
120 to use in situ observations from AWS and expand föhn detection with RACMO2 output to regions and times when AWS
121 observations are not available (Figure S1) (Table S1).

122 Föhn jet locations were identified using wind direction and strength during föhn events (Figure 2a) and by the
123 surface melt pattern during föhn (Figure 3b). The RACMO2 topography pixel size is 5.5 km which is sufficient to produce
124 the föhn jets identified on the LCIS (Elvidge et al., 2015), and allows for new föhn jet identification on the LAIS and LBIS
125 despite lack of direct observation. However, small-scale föhn winds funnelled through local canyons and mountain gaps

126 smaller than 5.5 km are not directly simulated. Therefore, we consider RACMO2 simulated estimates of surface melt caused
127 by föhn winds to be conservative and likely higher in regions where föhn winds are funnelled and concentrated.

128 **2.3 Ice shelf intercomparison analysis**

129 We split the ice shelves into areas shown in Figure 1a (Larsen A, Larsen B, SCAR inlet, Larsen C (north), and Larsen C) and
130 take the average of all model grid cells annually to create a climatology of surface melt, melt rate, melt hours, surface
131 temperature. We use a two-tailed t-test statistic to identify if the mean surface temperature and mean surface melt of both ice
132 shelves are statistically different from one another at the 95% confidence interval. We compare all ice shelves to the LBIS
133 because it was the most recent collapse event and is adjacent to collapsed and existing ice shelves. Qualitatively similar
134 results are obtained when comparing all ice shelves to the LAIS.

135 To compare ice shelf liquid water budgets we use a liquid-to-solid ratio (LSR) as a crude proxy for available firm air
136 content and can be estimated as,

$$137 \quad \quad \quad 138 \quad \quad \quad LSR = \frac{\text{Total liquid water (snowmelt + liquid precipitation)}}{\text{Total solid precipitation (snow)}} \quad (1)$$

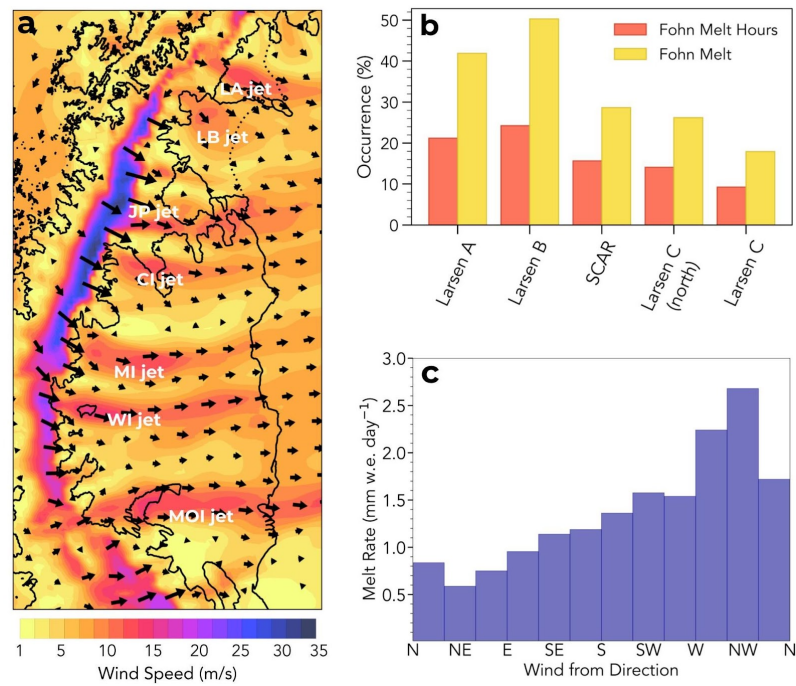
139
140 where areas with $LSR < 1$ represent an ice shelf that receives more solid precipitation than liquid water and is therefore less
141 likely to saturate with liquid water and form melt lakes than areas with $LSR > 1$.

142 **3 Results**

143 **3.1 Föhn jets and melt**

144 Using RACMO2 historical simulations, informed by a Machine Learning algorithm that is trained with AWS observations
145 (Laffin et al., 2021), we identify seven recurring föhn jets or “gap winds” that lead to high surface melt rates on the eastern
146 AP ice shelves (Figure 2a). Four of these jets (CI, MI, WI, MOI) have been studied using airborne observations and model
147 simulations (Grosvenor et al., 2014; Elvidge et al., 2015). The remaining three jets (LA, LB, and JP) are, to our knowledge,
148 identified here for the first time. Overall, winds from the west and northwest direction lead to increased surface melt rates
149 that can be up to 53% higher than melt when the wind is from other directions (Figure 2c) (van den Broeke (2005)).
150 Additionally, the degree to which föhn winds impact surface melt on each ice shelf varies depending on föhn jet location and
151 wind strength (Wiesenekker et al., 2018). These variations may provide insight into why SCAR inlet and the LCIS remain
152 intact while the LAIS and LBIS have collapsed other than the significant difference in annual surface temperature (Cook and
153 Vaughan (2009); Bozkurt et al., 2020; Carrasco et al., 2021).

154

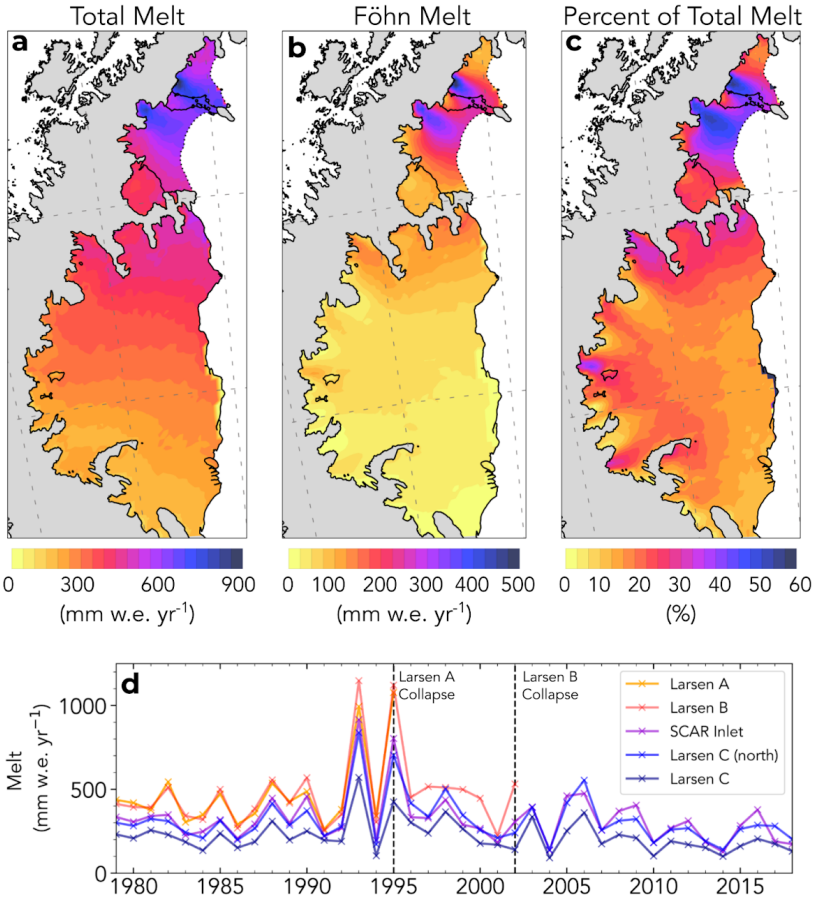


155 **Figure 2.** (a) The northern AP showing the RACMO2-simulated wind speed and direction vectors on January 24, 1995, just before the
156 collapse of the LAIS. Föhn jet locations are indicated with names. (b) RACMO2 annual average föhn melt hour percent of total melt
157 hours and föhn melt percent of total melt for each ice shelf from 1980-2002. (c) RACMO2 melt rate as a function of wind direction
158 averaged for all ice shelf regions on the AP from 1980-2002.

159

160 Surface melt production is more pronounced under the influence of föhn jets, particularly for the LA and LB jets
161 which produce 35.7% and 31.8% more melt respectively compared to regions not in the path of a föhn jet on each ice shelf
162 (Figure 3). Föhn-induced surface melt accounts for 42% of the total annual melt between 1979 and 2002 on the LAIS and
163 51% of total melt on the LBIS but only represents 21% and 25% of total melt hours on the LAIS and LBIS (Figure 2b, 3c).
164 In locations directly influenced by föhn jets, the mean annual föhn-induced melt was as high as 61% on the LAIS and 57%
165 on the LBIS of total annual melt. By contrast, föhn-induced melt accounts for only 25% of 1979-2002 total melt on SCAR
166 inlet and 17% on the LCIS. SCAR inlet is not directly impacted by a föhn jet, but still experiences clear skies and weak föhn
167 influence from the overall descending air during föhn events. The LCIS is affected by numerous föhn jets (CI, MI, WI,
168 MOI), accounting for up to 40% of the total annual melt in Cabinet and Whirlwind inlets, decreasing with distance east of
169 the AP mountains. The stark contrast in surface melt amount and fraction caused by föhn winds on collapsed vs. intact ice
170 shelves implicates föhn melt as a contributor to the LAIS and LBIS collapses. A clearer picture of the role of föhns emerges
171 after we examine föhn-induced melt extent and timing.

172 The spatial distribution and extent of surface melt influence ice shelf stability. Surface melt and melt lakes near the
 173 ice shelf terminus can lead to calving front collapse and structural instability for the remaining portion of the ice shelf
 174 (Depoorter et al., 2013; Pollard et al., 2015). Consistent with this mechanism, the LA and LB föhn jets impact a large spatial
 175 area of the LAIS and LBIS, and reach the ice shelf calving fronts (Figure 3b). SCAR Inlet lacks a strong föhn jet/influence
 176 and does not regularly experience largescale melt lakes even during high melt years (Figure 1b-f). This helps explain why
 177 SCAR Inlet is still intact, despite major structural changes observed after the collapse of the LBIS (Borstad et al., 2016; Qiao
 178 et al., 2020). LCIS on the other hand is impacted by four major jets and regularly experiences föhn-induced melt lakes,
 179 particularly in Cabinet inlet. However, the vast size of the LCIS does not allow the föhn-induced melt to reach the terminus.
 180 The föhn melt mechanism breaks down by mixing with cold air which reduces the intensity of the föhn jets from their peak
 181 at the base of the AP mountains to the calving front (Figure 3b). Having established that föhn winds significantly enhanced
 182 surface melt overall (Cape et al., 2015; Elvidge et al., 2015; Datta et al., 2019) and at the crucial calving front of LAIS and
 183 LBIS, we now examine the timing of föhn-induced melt events relative to collapse.



185 **Figure 3.** (a) RACMO2 average annual melt from 1980-2002. (b) RACMO2 average annual föhn wind-induced melt from 1980-2002. (c)
186 RACMO2 percent of total melt concurrent with föhn wind from 1980-2002. (d) RACMO2 time series of the mean annual surface melt on
187 each ice shelf from 1979-2018. Dashed vertical lines indicate the year in which each ice shelf collapsed. Note: The Larsen B curve often
188 overlaps the Larsen A curve.

189 **3.2 Coincidence of föhn winds with collapse**

190 **3.2.1 LAIS**

191 Three föhn wind events occurred on LAIS between January 18 and 27, 1995, overlapping with the initial phase of the LAIS
192 collapse that began on January 25 (Figure 4b) (Rott et al., 1998). These föhn events helped contribute to the collapse of the
193 ice shelf in two ways: (1) The west/northwest wind direction actively pushed or melted sea ice and fast ice away from the
194 calving front, allowing ocean waves to reach the terminus (Massom et al., 2018); (2) Enhanced surface melt rates caused by
195 the LA jet led to extensive melt lakes across the ice shelf that promoted large scale hydrofracture cascades when the ice shelf
196 terminus was breached (Banwell et al., 2013). The föhn wind events prior to and during collapse lasted an average of 3 days
197 each and produced increased surface melt greater than any other 9-day period from 1979-2018, with mean cumulative melt
198 of 268.5 mm w.e. or 25.2% of the total annual melt in the 1994/95 melt season. Total melt during the 1994/95 melt season
199 was 127% higher than an average year (474 mm w.e./yr) and the 9-day föhn wind event produced 57% of the total melt of an
200 average melt year. Therefore this 9-day föhn-induced melt event and melt year are clearly anomalous in the observational
201 record.

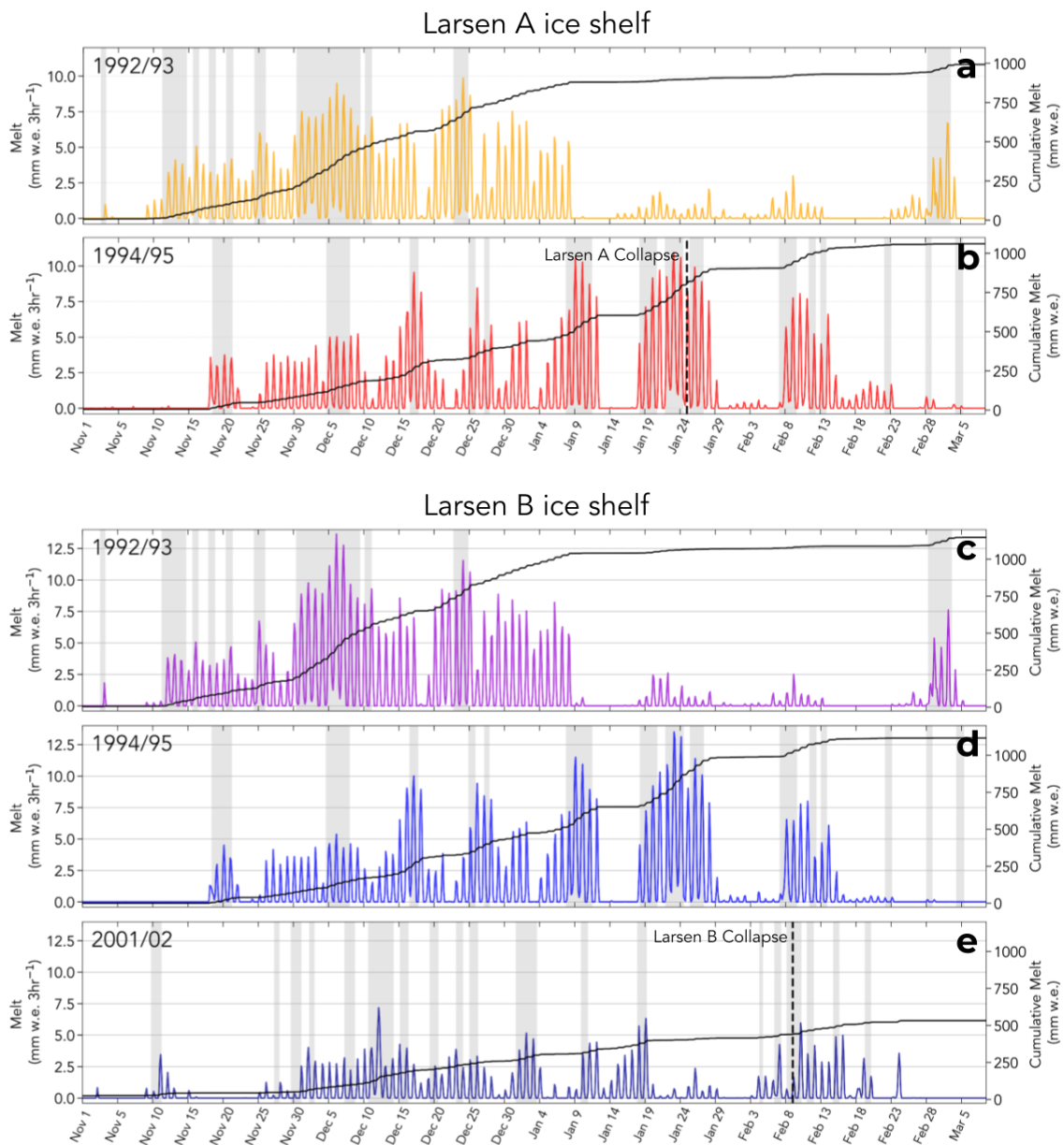
202 We next examine the contribution of föhn-generated melt to other observables implicated in the collapse, namely
203 surface liquid water, melt lake depth, and melt lake extent (Scambos et al., 2003). We estimate the spatial extent and depth of
204 melt lakes prior to collapse on the LAIS using satellite images of melt lake surface area combined with model-simulated
205 available liquid water volume. The cumulative spatial melt pattern between January 18 and 27, 1995 identifies significant
206 melt on the LAIS ranging from 157-356 mm w.e. (Figure S2a), varying spatially with the influence of the LA jet. Satellite
207 imagery of the LAIS during the collapse in progress show melt lakes were present (Figure S3) however because the collapse
208 had already begun, it is likely many of the lakes had drained or had been altered so estimating melt lake extent is not
209 possible. However, Advanced Very High-Resolution Radiometer (AVHRR) imagery on December 8, 1992, provides
210 high-resolution cloudless images of the ice shelf taken at the end of a similar föhn-induced melt event during a year when
211 melt was comparable to the 1994/95 melt season, therefore we consider this melt lake extent analogous to the 1994/95 melt
212 season (Figure 4a). We find the melt lake surface area was likely between 5.1%-10.8% (103 km^2 - 219 km^2) of the total LAIS
213 surface area (Figure S2b). Melt lake surface area is likely underestimated because the image was taken early in the 1992/93
214 melt season and does not easily identify small lakes or river systems. Liquid water pooling on the ice surface is modulated by
215 the local topography. If we assume all the available surface liquid water during the 9-day melt period, minus evaporation,

216 runoff, and refreeze, forms lakes that cover the same estimated surface area as the 1992/93 melt season, we can estimate melt
217 lake depth during the initial collapse. We find mean melt lake depth to be between 1.38-6.86 meters depending on lake
218 location and föhn influence, which exceeds the average lake depth of the LBIS lakes prior to collapse (1 meter) and the
219 critical lake depth that was identified in LBIS collapse modelling studies (3.5 m), especially under the influence of the LA jet
220 (Banwell et al., 2013).

221

222 **3.2.2 LBIS**

223 A föhn wind event coincided with the initial LBIS collapse on February 9, 2002, with two events just prior to collapse and
224 three additional events before complete collapse by March 17, 2002 (Figure 4c). Föhn events in the LBIS 2001/02 melt
225 season were relatively short, averaging less than 24 hours per event, and produced melt rates 27% higher than non-föhn melt
226 that year and 39% of the average föhn melt rate in all other years (Figure 4e). Similar to the LAIS collapse the off-coast wind
227 direction and enhanced surface melt rates during the föhn wind event helped push sea ice away from the calving front and
228 contributed to surface melt lakes that led to hydrofracture and collapse. Additionally, previous high melt rate föhn events
229 such as those in the 1992/93 and 1994/95 melt seasons likely preconditioned the LBIS through firn densification to support
230 melt lake formation, discussed in section 3.3.



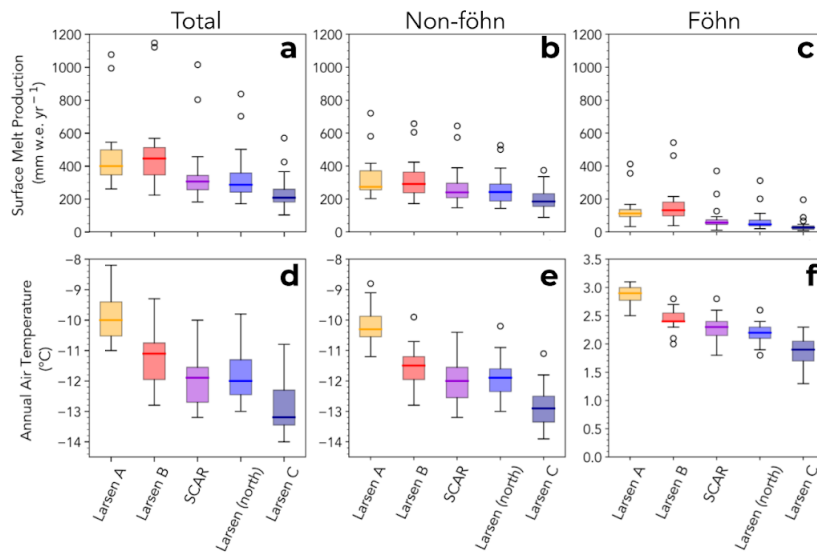
231

232 **Figure 4.** RACMO2 time series of surface melt production and cumulative melt during the Antarctic melt season averaged over the
 233 indicated ice shelf. Grey shading indicates the presence of föhn winds. (a) 1992/1993 LAIS. (b) 1994/1995 LAIS. (c) 1992/1993 LBIS. (d)
 234 1994/1995 LBIS. (e) 2001/2002 LBIS. *Note:* Surface melt that occurs after the collapse events indicated by the dashed vertical lines in (b)
 235 and (e) are estimates of melt quantity if the ice shelves did not disintegrate.

236 **3.3 Föhn melt and the surface liquid water budget**

237 To better understand the role that föhn winds play in AP ice shelf surface melt and stability we intercompare melt
238 climatologies and the surface liquid water budget of all major ice shelves. A comparison of collapsed with intact ice shelves
239 yields a clearer picture of the effects föhn winds have on ice shelf stability. We identify whether annual surface melt
240 production, melt rate, melt hours, and surface temperature variables from 1980-2002 are significantly different from the
241 LBIS (Figure 5 and corresponding two-tailed t-test statistics in Table S2). We compare to LBIS because it was centred
242 between other ice shelves and was the most recent to collapse. Total surface melt production on every ice shelf except LAIS
243 differs significantly from LBIS melt (Mean annual melt over the ice shelf area; LAIS-476 mm w.e., LBIS-479 mm w.e.,
244 SCAR-353 mm w.e., Larsen(north)-336 mm w.e., LCIS-238 mm w.e.) (Figure 5a), which is expected when we consider the
245 latitudinal location and mean annual air temperature (Figure 5d) (Table S2). However, when föhn-induced melt is subtracted
246 from total melt, the mean annual surface melt production on SCAR inlet and Larsen C (north) are not statistically different
247 from the LBIS (LAIS-337 mm w.e., LBIS-321 mm w.e., SCAR-286 mm w.e., Larsen(north)-278 mm w.e., LCIS-203 mm
248 w.e.) (Figure 5b). In other words, with the exception of föhn-induced melt (Figure 5c), melt production on SCAR Inlet and
249 LCIS are statistically indistinguishable at the 95% confidence interval from LBIS melt production. Föhn wind-induced
250 surface melt impacted collapsed ice shelves significantly more than extant ice shelves which further defines föhn melt as an
251 important contributor to LAIS and LBIS melt budget.

252 Our analysis of firn density or available firn pore space identifies significant differences in ice shelves that have
253 collapsed and those that remain intact. Firn densification occurs when the liquid water fills the pore space between snow/ice
254 crystals decreasing the air content in the firn, which forms refrozen ice layers that promote melt lake formation (Kuipers
255 Munneke et al., 2012; Polashenski et al., 2017). The liquid-to-solid ratio (LSR) is a crude proxy for available firn air content
256 with extant ice shelves (SCAR inlet, LCIS) have an LSR just above 1 for the period 1980-2002 if all surface melt is included
257 (Figure 6a). The LSR for LAIS and LBIS is also just above 1 for this period, though only if föhn-induced surface melt is
258 excluded. When surface melt caused by föhn wind is included, LSR exceeds 1.5 throughout extensive regions, including the
259 ice shelf margins, of the LAIS and LBIS. Thus the collapsed ice shelves experienced climatological LSRs significantly larger
260 than the extant ice shelves, mainly due to föhn-induced melt. This result suggests that föhn-induced melt helped precondition
261 the LAIS and LBIS to produce extensive melt lakes by long-term firn densification.

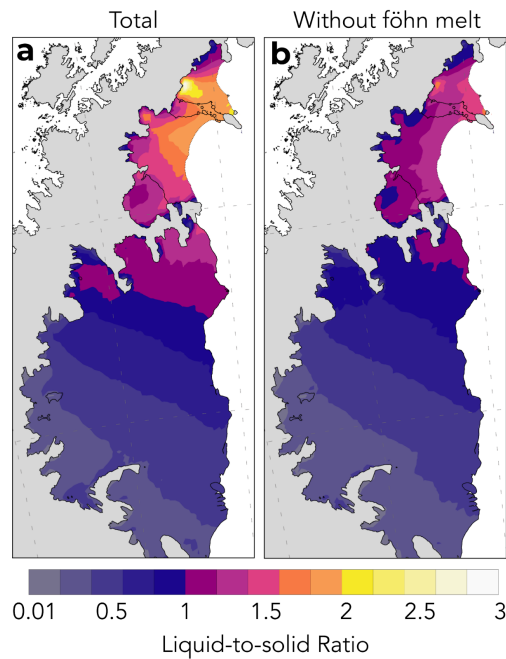


262

263 **Figure 5.** Box and whisker plots intercompare ice shelves with RACMO2-simulations from 1980-2002. Annual surface melt production
 264 (a) all melt, (b) non-föhn melt, (c) föhn-induced melt. (d) Mean annual air temperature, (e) air temperature without föhn winds, (f) air
 265 temperature during föhn winds. *Note:* the LAIS estimates are hypothetical after 1995, but are still resolved in the model simulations.

266

267



268

269 **Figure 6.** RACMO2 firn liquid-to-solid ratio or mean annual liquid water divided by mean annual frozen precipitation for (a) total melt
270 and (b) all liquid water except föhn-induced melt. *Note:* the LAIS estimates are hypothetical after 1995, but are still resolved in the model
271 simulations.

272 **4 Discussion**

273 The north/south temperature gradient present on the eastern AP ice shelves contributes to the differences in the ice shelf melt
274 regime (Figure 5). Warmer ice shelves can be more vulnerable to long-term thinning and retreat that accelerate disintegration
275 (Scambos et al., 2003; Morris and Vaughan (2003)). However, the temperature gradient alone does not explain the
276 substantial increase in surface melt on the LAIS and LBIS relative to more southerly ice shelves. Only with the addition of
277 föhn-induced surface melt (Figure 5c) do the LAIS and LBIS stand out significantly from the other eastern AP ice shelves
278 (Figure 5a,b). With that in mind, we have examined liquid water processes on the spatio-temporal scales pertinent to AP ice
279 shelf stability. For instance, the structural flow discontinuities or suture zones, where tributary glaciers merge together to
280 form an ice shelf, are mechanically weak points that impact stability (Sandhager et al., 2005; Glasser and Scambos (2008);
281 Glasser et al., 2009). These suture zones are further weakened through lateral shear depending on the difference in tributary
282 glacier flow. All ice shelves in the region are composed of numerous outflow glaciers sutured together, and while some
283 studies suggest this is a major contributor to ice shelf instability, only two of the ice shelves have collapsed (Borstad et al.,
284 2016; Glasser and Scambos (2008)). Further research suggests that marine accretion of ice on the bottom of the ice shelves,
285 specifically LCIS, may stabilise these suture zones, which may be why SCAR inlet has remained intact despite major rift
286 formation (McGrath et al., 2014; Borstad et al., 2016).

287 The timing of surface melt and melt enhanced by föhn winds within the melt season may also provide insight into
288 the fate of LAIS and LBIS, including why neither ice shelf collapsed in the anomalously strong 1992/93 melt season (Figure
289 3d). Pore space within the upper snow and firn layers buffers surface melt before lakes begin to form (Polashenski et al.,
290 2017). Late season melt is more likely to form surface melt lakes because meltwater from the preceding fall, winter, and
291 spring has partially or completely filled available pore space. On both the LAIS and LBIS, 92% of surface melt during the
292 1992/93 melt season occurred before January 9th when there was more pore space to buffer the anomalous surface melt than
293 at the onsets of their collapses in late January 1995 and early February 2002, respectively (Figure 4a, c). Melt lakes were
294 present on both ice shelves throughout the 1992/93 melt season, though melt production slowed dramatically after
295 mid-January, 1993 (Scambos et al., 2000). The high melt rates in late November and early December 1992 on the LAIS were
296 perhaps too early in the melt season, and after too many years of nominal melt, to form substantial melt lakes and trigger
297 hydrofracture that season. Nevertheless, the 1992/93 melt could have preconditioned the shelf for collapse in January 1995.
298 The LBIS collapse began in February 2002 after the surface melt had returned to nominal, 1980s levels for six years. How
299 much pore space had recovered during those six years is unknown, and an important question for future research. Satellite

300 images of surface melt lakes indicate 11% of the ice shelf was covered in melt lakes prior to collapse (Glasser and Scambos
301 (2008)). However, the preceding melt year (2000/2001) had low melt and high precipitation, which added additional snow
302 mass to the unstable ice shelf (Leeson et al., 2017).

303 Another possible reason collapse did not occur in the 92/93 melt season or other years prior to collapse was a
304 possible misalignment of the four prerequisites for rapid collapse theorised by Massom et al., (2018). An AVHRR image of
305 the LAIS taken on December 8, 1992, just after a series of major föhn wind events that lead to 252 mm w.e. of surface melt
306 in the 8 days prior to the image (Figure 4a), show significant melt lakes across the LAIS, which make hydrofracture cascades
307 possible. However, in the same image, sea ice/melange are shown to be at the calving front, protecting the front from large
308 ocean waves that could trigger collapse. It may have been too early in the melt season to have substantial gaps in sea ice, the
309 ocean temperature may have been too cold, ocean circulation could have helped stabilise the sea ice at the front, the föhn winds
310 speed could have been too weak to push the ice away or may have been in the wrong direction, all of which could have not
311 allowed a proper trigger for collapse even though substantial melt ponds were present. Even if there were years or instances
312 that sea ice extent was low and substantial melt lakes were present, there could have been a lack of large period ocean swells
313 that are thought to trigger collapse.

314 Regardless of other possible contributors to ice shelf instability not considered here (e.g., basal warming),
315 föhn-induced surface melt and associated melt lakes, and the off-coast wind direction likely played an important role in
316 pushing the LAIS and LBIS past a structural tipping point. The estimated surface melt lake depth caused by the 9-day föhn
317 melt event on the LAIS surpassed the critical melt lake depth of stability identified by model studies and satellite-derived
318 lake depths before the collapse of the LBIS (Banwell et al., 2013). The LAIS was likely the same thickness (200m) or
319 thinner at the time of collapse so the estimate of critical surface lake depth for the LBIS that is applied to the LAIS may
320 reflect an upper limit of melt lake depth of stability for the LAIS. Melt lake depth is likely underestimated because our
321 estimation only accounts for melt during the 9-day melt event. Melt before this time period already exceeded an average melt
322 year by 23% (118 mm w.e.) so melt lakes probably already existed.

323 5 Conclusions

324 The converging lines of evidence in these results show that observed and inferred föhn-driven melt is present in sufficient
325 amounts, and at the right locations and times, to cause extensive surface melt lakes, while the off-coast föhn wind direction
326 pushed sea ice away from the calving front. The fact that the LAIS and LBIS collapsed catastrophically within weeks and
327 not through long-term thinning and retreat like other ice shelves (Prince Gustav, Wordie) suggests sudden disintegration is
328 anomalous and requires forcings to match vulnerabilities (Scambos et al., 2003). We conclude that föhn winds and the
329 associated surface melt played a significant role in the collapses of the LAIS and LBIS, while extant AP ice shelves are not

likely to collapse from föhn-induced melt and hydrofracture in today's current climate. We have come to these conclusions with the following forms of evidence:

- First, both the LAIS and LBIS are impacted by powerful melt-inducing föhn jets that affect a large spatial portion of each ice shelf and reach the ice shelf terminus. Surface melt and melt lakes near the ice shelf terminus can lead to calving front collapse and structural instability for the remaining portion of the ice shelves (Depoorter et al., 2013; Pollard et al., 2015). Extant ice shelves are either not directly affected by a föhn jet, are too vast to have any significant effect near the terminus, or are too far south to experience major melt events.
- Second, strong föhn winds were present prior to and during collapse for the LAIS and LBIS. A series of three föhn events on the LAIS lasted nine days total and produced over 25% of the total annual melt for the 1994/95 melt season, while föhn was present prior to and during the collapse of the LBIS which enhanced surface melt rates. Enhanced melt, filled new and existing melt lakes above the critical (1 meter) melt lake depth of stability. The föhn winds on both ice shelves actively pushed sea ice away from the calving front allowing large period ocean swells to trigger large scale hydrofracture cascades exacerbated by extensive surface melt and originated from the ice shelf terminus.
- Third, in the absence of föhn wind-induced melt, the surface liquid budgets of collapsed and intact ice shelves are climatically similar, which points to föhn winds as a driver of increased surface melt and extensive melt lakes on collapsed ice shelves. The additional föhn induced-melt on the LAIS and LBIS compared to intact ice shelves helped precondition the LAIS and LBIS to produce extensive melt lakes by long-term firn densification.

This research clarifies the roles of föhn-induced melt for collapsed and extant ice shelves. Future analyses of these ice shelf collapse events using advanced firn density models coupled with ice-ocean-atmospheric coupled simulations may be useful to better understand the role of surface melt in ice shelf instability. Further, the AP föhn wind regime has remained stable over the past half-century (Laffin et al., 2021) which points to enhanced surface temperatures and increased liquid phase precipitation as more important contributors to the future surface liquid budget on remaining ice shelves and is an important area of future research (Bozkurt et al., 2020; Bozkurt et al., 2021). However, changes in climate drivers such as the Southern Annular Mode (SAM), which influences the north-south movement of the westerlies in the region, may alter the temperature and föhn occurrence that will likely enhance surface melt in locations farther south, and therefore make northern southern ice shelves more vulnerable (Abram et al., 2014; Zheng et al., 2013; Lim et al., 2016;). Nevertheless, this research highlights a new understanding behind surface melt mechanisms for ice shelf collapse and suggests that extant ice shelves in the region may remain stable so long as surface liquid water from melt and precipitation remains within historical bounds.

362

363 *Author contributions.* M.K.L and C.S.Z designed the study. M.V.W. and S.M. curated the model simulation output and
364 surface observations. M.K.L performed statistical data analysis. M.K.L. wrote the article with valuable input from all
365 authors.

366

367 *Competing interests.* The authors declare no conflict of interest.

368

369 *Acknowledgments.* MKL was supported by the National Science Foundation (NRT-1633631) and NASA AIST
370 (80NSSC17K0540). CSZ gratefully acknowledges support from the DOE BER ESM and SciDAC programs
371 (DE-SC0019278, LLNL-B639667, LANL-520117). JMW acknowledges support by PROTECT and was partly funded by
372 the NWO (Netherlands Organisation for Scientific Research) VENI grant VI.Veni.192.083. We thank Dr. Helmut Rott for
373 generously providing detailed in-person observations of the LAIS months before collapse. We also thank the Institute for
374 Marine and Atmospheric research Utrecht (IMAU) for providing RACMO2 output. RACMO2 model data are available by
375 request at <https://www.projects.science.uu.nl/iceclimate/models/antarctica.php>, however, a subset (2001-2018) of the data are
376 hosted online at <https://zenodo.org/record/3677642#.X-pXAFNKjUI>.

377 **References**

378 Abram, N. J., Mulvaney, R., Vimeux, F., Phipps, S. J., Turner, J. and England, M. H.: Evolution of the Southern Annular
379 Mode during the past millennium, *Nat. Clim. Chang.*, 4(7), 564–569, doi:10.1038/nclimate2235, 2014.

380 Adusumilli, S., Fricker, H. A., Siegfried, M. R., Padman, L., Paolo, F. S. and Ligtenberg, S. R. M.: Variable Basal Melt Rates
381 of Antarctic Peninsula Ice Shelves, 1994–2016, *Geophys. Res. Lett.*, 45(9), 4086–4095, doi:10.1002/2017GL076652,
382 2018.

383 Alley, K. E., Scambos, T. A., Miller, J. Z., Long, D. G. and MacFerrin, M.: Quantifying vulnerability of Antarctic ice shelves
384 to hydrofracture using microwave scattering properties, *Remote Sens. Environ.*, 210, 297–306,
385 doi:10.1016/j.rse.2018.03.025, 2018.

386 Banwell, A. F., Caballero, M., Arnold, N. S., Glasser, N. F., Cathles, L. Mac and MacAyeal, D. R.: Supraglacial lakes on the
387 Larsen B ice shelf, Antarctica, and at Paakitsoq, West Greenland: A comparative study, *Ann. Glaciol.*, 55(66), 1–8,
388 doi:10.3189/2014AoG66A049, 2014.

389 Banwell, A. F., MacAyeal, D. R. and Sergienko, O. V.: Breakup of the Larsen B Ice Shelf triggered by chain reaction
390 drainage of supraglacial lakes, *Geophys. Res. Lett.*, 40(22), 5872–5876, doi:10.1002/2013GL057694, 2013.

391 Banwell, A. F., Willis, I. C., Macdonald, G. J., Goodsell, B. and MacAyeal, D. R.: Direct measurements of ice-shelf flexure
392 caused by surface meltwater ponding and drainage, *Nat. Commun.*, 10(1), doi:10.1038/s41467-019-08522-5, 2019.

393 Banwell, A. F., Willis, I. C., MacDonald, G. J., Goodsell, B., Mayer, D. P., Powell, A. and MacAyeal, D. R.: Calving and
 394 rifting on the McMurdo Ice Shelf, Antarctica, *Ann. Glaciol.*, 58(75), 78–87, doi:10.1017/aog.2017.12, 2017.

395 Bell, R. E., Banwell, A. F., Trusel, L. D. and Kingslake, J.: Antarctic surface hydrology and impacts on ice-sheet mass
 396 balance, *Nat. Clim. Chang.*, 8(12), 1044–1052, doi:10.1038/s41558-018-0326-3, 2018.

397 Bevan, S. L., Luckman, A., Hubbard, B., Kulessa, B., Ashmore, D., Kuipers Munneke, P., O’Leary, M., Booth, A., Sevestre,
 398 H. and McGrath, D.: Centuries of intense surface melt on Larsen C Ice Shelf, *Cryosphere*, doi:10.5194/tc-11-2743-2017,
 399 2017.

400 Borstad, C., Khazendar, A., Scheuchl, B., Morlighem, M., Larour, E. and Rignot, E.: A constitutive framework for predicting
 401 weakening and reduced buttressing of ice shelves based on observations of the progressive deterioration of the remnant
 402 Larsen B Ice Shelf, *Geophys. Res. Lett.*, 43(5), 2027–2035, doi:10.1002/2015GL067365, 2016.

403 Bozkurt, D., Rondanelli, R., Marín, J. C. and Garreaud, R.: Foehn Event Triggered by an Atmospheric River Underlies
 404 Record-Setting Temperature Along Continental Antarctica, *J. Geophys. Res. Atmos.*, doi:10.1002/2017JD027796, 2018.

405 Bozkurt, D., Bromwich, D. H., Carrasco, J., Hines, K. M., Maureira, J. C. and Rondanelli, R.: Recent Near-surface
 406 Temperature Trends in the Antarctic Peninsula from Observed, Reanalysis and Regional Climate Model Data, *Adv.*
 407 *Atmos. Sci.*, 37(5), 477–493, doi:10.1007/s00376-020-9183-x, 2020.

408 Bozkurt, D., Bromwich, D. H., Carrasco, J. and Rondanelli, R.: Temperature and precipitation projections for the Antarctic
 409 Peninsula over the next two decades: contrasting global and regional climate model simulations, *Clim. Dyn.*,
 410 doi:10.1007/s00382-021-05667-2, 2021.

411 Braun, M. and Humbert, A.: Recent retreat of wilkins ice shelf reveals new insights in ice shelf breakup mechanisms, *IEEE*
 412 *Geosci. Remote Sens. Lett.*, 6(2), 263–267, doi:10.1109/LGRS.2008.2011925, 2009.

413 Burton, J. C., Cathles, L. Mac and Wilder, W. G.: The role of cooperative iceberg capsize in ice-shelf disintegration, *Ann.*
 414 *Glaciol.*, 54(63), 84–90, doi:10.3189/2013AoG63A436, 2013.

415 Cape, M. R., Vernet, M., Skvarca, P., Marinsek, S., Scambos, T. and Domack, E.: Foehn winds link climate-driven warming
 416 to ice shelf evolution in Antarctica, *J. Geophys. Res.*, doi:10.1002/2015JD023465, 2015.

417 Carrasco, J. F., Bozkurt, D. and Cordero, R. R.: A review of the observed air temperature in the Antarctic Peninsula. Did the
 418 warming trend come back after the early 21st hiatus?, *Polar Sci.*, 28, doi:10.1016/j.polar.2021.100653, 2021.

419 Cook, A. J. and Vaughan, D. G.: Ice shelf changes on the Antarctic Peninsula Overview of areal changes of the ice shelves
 420 on the Antarctic Peninsula over the past 50 years Ice shelf changes on the Antarctic Peninsula, *TCD*, 3, 579–630
 421 [online] Available from: www.the-cryosphere-discuss.net/3/579/2009/, 2009.

422 Datta, R. T., Tedesco, M., Fettweis, X., Agosta, C., Lhermitte, S., Lenaerts, J. T. M. and Wever, N.: The Effect of
 423 Foehn Induced Surface Melt on Firn Evolution Over the Northeast Antarctic Peninsula, *Geophys. Res. Lett.*,
 424 2018GL080845, doi:10.1029/2018GL080845, 2019.

425 Depoorter, M. A., Bamber, J. L., Griggs, J. A., Lenaerts, J. T. M., Ligtenberg, S. R. M., Van Den Broeke, M. R. and Moholdt,
 426 G.: Calving fluxes and basal melt rates of Antarctic ice shelves, *Nature*, 502(7469), 89–92, doi:10.1038/nature12567,
 427 2013.

428 Doake, C. S. M., Corr, H. F. J., Rott, H., Skvarca, P. and Young, N. W.: Breakup and conditions for stability of the northern
 429 Larsen Ice Shelf, Antarctica, *Nature*, 391, 778–780, 1988.

430 Elvidge, A. D., Kuipers Munneke, P., King, J. C., Renfrew, I. A. and Gilbert, E.: Atmospheric Drivers of Melt on Larsen C
 431 Ice Shelf: Surface Energy Budget Regimes and the Impact of Foehn, *J. Geophys. Res. Atmos.*, 125(17),
 432 doi:10.1029/2020JD032463, 2020.

433 Elvidge, A. D., Renfrew, I. A., King, J. C., Orr, A., Lachlan-Cope, T. A., Weeks, M. and Gray, S. L.: Foehn jets over the
 434 Larsen C Ice Shelf, Antarctica, *Q. J. R. Meteorol. Soc.*, 141(688), 698–713, doi:10.1002/qj.2382, 2015.

435 Glasser, N. F. and Scambos, T. A.: A structural glaciological analysis of the 2002 Larsen B ice-shelf collapse, *J. Glaciol.*,
 436 54(184), 3–16, doi:10.3189/002214308784409017, 2008.

437 Glasser, N. F., Kulesa, B., Luckman, A., Jansen, D., King, E. C., Sammonds, P. R., Scambos, T. A. and Jezek, K. C.:
 438 Surface structure and stability of the Larsen C ice shelf, *Antarctic Peninsula*, 2009.

439 Grosvenor, D. P., King, J. C., Choularton, T. W. and Lachlan-Cope, T.: Downslope föhn winds over the antarctic peninsula
 440 and their effect on the larsen ice shelves, *Atmos. Chem. Phys.*, 14(18), 9481–9509, doi:10.5194/acp-14-9481-2014,
 441 2014.

442 Gudmundsson, G. H.: Ice-shelf buttressing and the stability of marine ice sheets, *Cryosphere*, 7(2), 647–655,
 443 doi:10.5194/tc-7-647-2013, 2013. Holland, P. R., Corr, H. F. J., Pritchard, H. D., Vaughan, D. G., Arthern, R. J., Jenkins,
 444 A. and Tedesco, M.: The air content of Larsen Ice Shelf, *Geophys. Res. Lett.*, doi:10.1029/2011GL047245, 2011.

445 King, J. C., Gadian, A., Kirchgaessner, A., Kuipers Munneke, P., Lachlan-Cope, T. A., Orr, A., Reijmer, C., van den Broeke,
 446 M. R., van Wessem, J. M. and Weeks, M.: Validation of the summertime surface energy budget of Larsen C Ice Shelf
 447 (Antarctica) as represented in three high-resolution atmospheric models, *J. Geophys. Res.*, 120(4), 1335–1347,
 448 doi:10.1002/2014JD022604, 2015.

449 King, J. C., Kirchgaessner, A., Bevan, S., Elvidge, A. D., Kuipers Munneke, P., Luckman, A., Orr, A., Renfrew, I. A. and van
 450 den Broeke, M. R.: The Impact of Föhn Winds on Surface Energy Balance During the 2010–2011 Melt Season Over
 451 Larsen C Ice Shelf, Antarctica, *J. Geophys. Res. Atmos.*, doi:10.1002/2017JD026809, 2017.

452 Kirchgaessner, A., King, J. C. and Anderson, P. S.: The Impact of Föhn Conditions Across the Antarctic Peninsula on Local
 453 Meteorology Based on AWS Measurements, *J. Geophys. Res. Atmos.*, 126(4), doi:10.1029/2020JD033748, 2021.

454 Kuipers Munneke, P., Luckman, A. J., Bevan, S. L., Smeets, C. J. P. P., Gilbert, E., van den Broeke, M. R., Wang, W.,
 455 Zender, C., Hubbard, B., Ashmore, D., Orr, A., King, J. C. and Kulesa, B.: Intense Winter Surface Melt on an Antarctic
 456 Ice Shelf, *Geophys. Res. Lett.*, doi:10.1029/2018GL077899, 2018.

Kuipers Munneke, P., Van Den Broeke, M. R., King, J. C., Gray, T. and Reijmer, C. H.: Near-surface climate and surface
 energy budget of Larsen C ice shelf, Antarctic Peninsula, Cryosphere, 6(2), 353–363, doi:10.5194/tc-6-353-2012, 2012.

Laffin, M. K., Zender, C. S., Singh, S., Van Wessem, J. M., Smeets, C. J. P. P. and Reijmer, C. H.: Climatology and
 Evolution of the Antarctic Peninsula Föhn Wind-Induced Melt Regime From 1979–2018, J. Geophys. Res. Atmos.,
 126(4), doi:10.1029/2020JD033682, 2021.

Larour, E., Rignot, E., Poinelli, M. and Scheuchl, B.: Physical processes controlling the rifting of Larsen C Ice Shelf,
 Antarctica, prior to the calving of iceberg A68, Proc. Natl. Acad. Sci. U. S. A., 118(40), doi:10.1073/pnas.2105080118,
 2021.

Leeson, A. A., Forster, E., Rice, A., Gourmelen, N. and van Wessem, J. M.: Evolution of Supraglacial Lakes on the Larsen B
 Ice Shelf in the Decades Before it Collapsed, Geophys. Res. Lett., 47(4), doi:10.1029/2019GL085591, 2020.

Leeson, A. A., Van Wessem, J. M., Ligtenberg, S. R. M., Shepherd, A., Van Den Broeke, M. R., Killick, R., Skvarca, P.,
 Marinsek, S. and Colwell, S.: Regional climate of the Larsen B embayment 1980-2014, J. Glaciol., 63(240), 683–690,
 doi:10.1017/jog.2017.39, 2017.

Lenaerts, J. T. M., Lhermitte, S., Drews, R., Ligtenberg, S. R. M., Berger, S., Helm, V., Smeets, C. J. P. P., Broeke, M. R. V.
 Den, Van De Berg, W. J., Van Meijgaard, E., Eijkelboom, M., Eisen, O. and Pattyn, F.: Meltwater produced by
 wind-albedo interaction stored in an East Antarctic ice shelf, Nat. Clim. Chang., doi:10.1038/nclimate3180, 2017.

Lhermitte, S., Sun, S., Shuman, C., Wouters, B., Pattyn, F., Wuite, J., Berthier, E. and Nagler, T.: Damage accelerates ice
 shelf instability and mass loss in Amundsen Sea Embayment, Sci. Libr. Ser., 117,
 doi:10.1073/pnas.1912890117/-DCSupplemental.y, 2020.

Lim, E. P., Hendon, H. H., Arblaster, J. M., Delage, F., Nguyen, H., Min, S. K. and Wheeler, M. C.: The impact of the
 Southern Annular Mode on future changes in Southern Hemisphere rainfall, Geophys. Res. Lett., 43(13), 7160–7167,
 doi:10.1002/2016GL069453, 2016.

Luckman, A., Elvidge, A., Jansen, D., Kulesa, B., Kuipers Munneke, P., King, J. and Barrand, N. E.: Surface melt and
 ponding on Larsen C Ice Shelf and the impact of föhn winds, Antarct. Sci., doi:10.1017/S0954102014000339, 2014.

Massom, R. A., Scambos, T. A., Bennetts, L. G., Reid, P., Squire, V. A. and Stammerjohn, S. E.: Antarctic ice shelf
 disintegration triggered by sea ice loss and ocean swell, Nature, 558(7710), 383–389, doi:10.1038/s41586-018-0212-1,
 2018.

McGrath, D., Steffen, K., Holland, P. R., Scambos, T., Rajaram, H., Abdalati, W. and Rignot, E.: The structure and effect of
 suture zones in the Larsen C Ice Shelf, Antarctica, J. Geophys. Res. Earth Surf., 119(3), 588–602,
 doi:10.1002/2013JF002935, 2014.

Morris, E. M. and Vaughan, D. G.: Spatial and Temporal Variation of Surface Temperature on the Antarctic Peninsula and
 the Limit of Viability of Ice Shelves, Antarct. Res. Ser., 79, 61–68, doi:10.1029/079ARS05, 2003.

489 Mulvaney, R., Abram, N. J., Hindmarsh, R. C. A., Arrowsmith, C., Fleet, L., Triest, J., Sime, L. C., Alemany, O. and Foord,
490 S.: Recent Antarctic Peninsula warming relative to Holocene climate and ice-shelf history, *Nature*, 489(7414), 141–144,
491 doi:10.1038/nature11391, 2012.

492 Munneke, P. K., Ligtenberg, S. R. M., Van Den Broeke, M. R. and Vaughan, D. G.: Firn air depletion as a precursor of
493 Antarctic ice-shelf collapse, *J. Glaciol.*, 60(220), 205–214, doi:10.3189/2014JoG13J183, 2014.

494 Polashenski, C., Golden, K. M., Perovich, D. K., Skyllingstad, E., Arnsten, A., Stwertka, C. and Wright, N.: Percolation
495 blockage: A process that enables melt pond formation on first year Arctic sea ice, *J. Geophys. Res. Ocean.*, 122(1),
496 413–440, doi:10.1002/2016JC011994, 2017.

497 Pollard, D., DeConto, R. M. and Alley, R. B.: Potential Antarctic Ice Sheet retreat driven by hydrofracturing and ice cliff
498 failure, *Earth Planet. Sci. Lett.*, 412, 112–121, doi:10.1016/j.epsl.2014.12.035, 2015.

499 Pritchard, H. D., Ligtienberg, S. R. M., Fricker, H. A., Vaughan, D. G., Van Den Broeke, M. R. and Padman, L.: Antarctic
500 ice-sheet loss driven by basal melting of ice shelves, *Nature*, 484(7395), 502–505, doi:10.1038/nature10968, 2012.

501 Qiao, G., Li, Y., Guo, S. and Ye, W.: Evolving instability of the scar inlet ice shelf based on sequential landsat images
502 spanning 2005-2018, *Remote Sens.*, 12(1), doi:10.3390/RS12010036, 2020.

503 Rack, W. and Rott, H.: Pattern of retreat and disintegration of the Larsen B ice shelf, Antarctic Peninsula, *Ann. Glaciol.* , 39,
504 505–510 [online] Available from: <https://www.cambridge.org/core>., 2004.

505 Rignot, E., Jacobs, S., Mouginot, B. and Scheuchl, B.: Ice-Shelf Melting Around Antarctica, *Science* (80-.), 341(6143),
506 263–266, doi:10.1126/science.1237966, 2013. Rignot, E., Casassa, G., Gogineni, P., Krabill, W., Rivera, A. and Thomas,
507 R.: Accelerated ice discharge from the Antarctic Peninsula following the collapse of Larsen B ice shelf, *Geophys. Res.*
508 *Lett.*, 31(18), doi:10.1029/2004GL020697, 2004.

509 Robel, A. A. and Banwell, A. F.: A Speed Limit on Ice Shelf Collapse Through Hydrofracture, *Geophys. Res. Lett.*, 46(21),
510 12092–12100, doi:10.1029/2019GL084397, 2019. Rott, H., Rack, W., Nagler, T. and Skvarca, P.: Climatically induced
511 retreat and collapse of norther Larsen Ice Shelf, Antarctic Peninsula, *Ann. Glaciol.*, 27, 86–92,
512 doi:10.3189/s0260305500017262, 1998.

513 Sandhäger, H., Rack, W. and Jansen, D.: Model investigations of Larsen B Ice Shelf dynamics prior to the breakup. [online]
514 Available from: <http://www.uib.no/People/ngfls/frisp/Rep16/sandhageretal.pdf>, 2005.

515 Scambos, T. A., Bohlander, J. A., Shuman, C. A. and Skvarca, P.: Glacier acceleration and thinning after ice shelf collapse in
516 the Larsen B embayment, Antarctica, *Geophys. Res. Lett.*, 31(18), doi:10.1029/2004GL020670, 2004.

517 Scambos, T. A., Hulbe, C., Fahnestock, M. and Bohlander, J.: The link between climate warming and break-up of ice shelves
518 in the Antarctic Peninsula, *J. Glaciol.*, 46(154), 516–530, doi:10.3189/172756500781833043, 2000.

519 Scambos, T., Hulbe, C. and Fahnestock, M.: Climate-Induced Ice Shelf Disintegration in the Antarctic Peninsula, pp. 79–92.,
520 2003.

521 Schodlok, M. P., Menemenlis, D. and Rignot, E. J.: Ice shelf basal melt rates around Antarctica from simulations and
522 observations, *J. Geophys. Res. Ocean.*, 121(2), 1085–1109, doi:10.1002/2015JC011117, 2016.

523 Trusel, L. D., Frey, K. E., Das, S. B., Karnauskas, K. B., Kuipers Munneke, P., Van Meijgaard, E. and Van Den Broeke, M.
524 R.: Divergent trajectories of Antarctic surface melt under two twenty-first-century climate scenarios, *Nat. Geosci.*,
525 8(12), 927–932, doi:10.1038/ngeo2563, 2015.

526 Trusel, L. D., Frey, K. E., Das, S. B., Munneke, P. K. and Van Den Broeke, M. R.: Satellite-based estimates of Antarctic
527 surface meltwater fluxes, *Geophys. Res. Lett.*, 40(23), 6148–6153, doi:10.1002/2013GL058138, 2013.

528 Turton, J. V., Kirchgaessner, A., Ross, A. N. and King, J. C.: Does high-resolution modelling improve the spatial analysis of
529 föhn flow over the Larsen C Ice Shelf?, *Weather*, 72(7), doi:10.1002/wea.3028, 2017.

530 Turton, J. V., Kirchgaessner, A., Ross, A. N. and King, J. C.: The spatial distribution and temporal variability of föhn winds
531 over the Larsen C ice shelf, Antarctica, *Q. J. R. Meteorol. Soc.*, doi:10.1002/qj.3284, 2018.

532 van den Broeke, M.: Strong surface melting preceded collapse of Antarctic Peninsula ice shelf, *Geophys. Res. Lett.*, 32(12),
533 1–4, doi:10.1029/2005GL023247, 2005.

534 Vaughan, D. G., Marshall, G. J., Connolley, W. M., Parkinson, C., Mulvaney, R., Hodgson, D. A., King, J. C., Pudsey, C. J.
535 and Turner, J.: Recent rapid regional climate warming on the Antarctic Peninsula, *Clim. Change*, 60(3), 243–274,
536 doi:10.1023/A:1026021217991, 2003.

537 Wang, W., Zender, C. S., van As, D., Fausto, R. S. and Laffin, M. K.: Greenland Surface Melt Dominated by Solar and
538 Sensible Heating, *Geophys. Res. Lett.*, 48(7), doi:10.1029/2020GL090653, 2021.

539 Wiesenekker, J. M., Munneke, P. K., van den Broeke, M. R. and Paul Smeets, C. J. P.: A multidecadal analysis of Föhn
540 winds over Larsen C ice shelf from a combination of observations and modeling, *Atmosphere (Basel)*, 9(5),
541 doi:10.3390/atmos9050172, 2018.

542 Zheng, F., Li, J., Clark, R. T. and Nnamchi, H. C.: Simulation and projection of the Southern Hemisphere annular mode in
543 CMIP5 models, *J. Clim.*, 26(24), 9860–9879, doi:10.1175/JCLI-D-13-00204.1, 2013.